A Compact DC Model for PEDOT-Based Organic Electrochemical Transistors (OECTs)

Benito González, Laia Masip, Marc Lázaro, Ramón Villarino, David Girbau, *Senior Member, IEEE*, and Antonio Lázaro, *Senior Member, IEEE*

***Abstract*— In this article, a compact model of the dc characteristics of organic electrochemical transistors (OECTs) is proposed. Starting from the output characteristics, the transconductance in the saturation regime is modeled after the output conductance in the saturation regime is reduced to very low values. For this purpose, a previously justified integrable bell-shaped function is used, based on which the transfer characteristics in the saturation regime are determined. Since the drain current due to hopping diminishes in the linear regime, the model is based on the gradual channel approximation and constant hole mobility and gate capacitance at this regime. Six parameters are required for dc modeling, which can be obtained in a straightforward way from the transconductance and transfer characteristics in the saturation regime, and the output characteristics. A good agreement between the modeled and measured data is achieved. The proposed compact model stands out in terms of its simplicity and rapid determination of its parameters and can be easily incorporated into circuit simulators.**

***Index Terms*— Circuit simulator, compact model, dc characterization, organic electrochemical transistor (OECT), peak transconductance.**

I. Introduction

AN ORGANIC electrochemical transistor (OECT) is a type of organic thin-film transistor (OTFT) that has attracted increasing amounts of attention in the area of chemical and biological sensing applications [1], [2], digital logic [3], and neuromorphic engineering [4].

Received 11 April 2024; revised 28 June 2024 and 8 September 2024; accepted 23 September 2024. Date of publication 7 October 2024; date of current version 24 October 2024. This work was supported by Spanish Ministerio de Ciencia e Innovación and Agencia Estatal de Investigación through MCIN/AEI/10.13039/501100011033 under Project PID2021-1223990B-I00, Project TED2021-130307B-I00, and Project PRE2019-089028. The review of this article was arranged by Editor B. Iñiguez. *(Corresponding author: Benito González.)*

Benito González is with the Institute for Applied Microelectronics, Universidad de Las Palmas de Gran Canaria (ULPGC), Campus Universitario de Tafira, 35017 Las Palmas, Spain (e-mail: benito@iuma.ulpgc.es).

Laia Masip, Marc Lázaro, Ramón Villarino, David Girbau, and Antonio Lázaro are with the Department of Electronics, Electrics and Automatic Control Engineering, Escola Tècnica Superior d'Enginyeria, Universitat Rovira i Virgili, 43007 Tarragona, Spain (e-mail: laia.masip@urv.cat; marc.lazaro@urv.cat; ramon.villarino@urv.cat; david.girbau@urv.cat; antonioramon.lazaro@urv.cat).

Color versions of one or more figures in this article are available at https://doi.org/10.1109/TED.2024.3469170.

Digital Object Identifier 10.1109/TED.2024.3469170

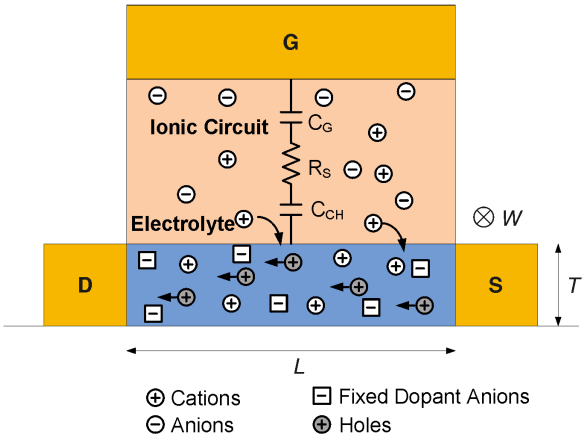

Fig. 1. Typical diagram of an OECT, showing the source (S), drain (D), electrolyte, and gate (G). In this diagram, the gate is considered located over the channel. The ionic circuit is represented by a series *RC* circuit and the electronic circuit by a variable channel resistance controlled by the gate voltage. *L*, *W*, and *T* are the channel length, width, and thickness, respectively.

The typical structure of an OECT is shown in Fig. 1, where L, W, and T are the channel length, width, and thickness, respectively. It consists of a metallic source, drain and gate electrodes, and a polymer semiconductor channel between the source and the drain. The conducting polymer film is in contact with an electrolyte, in which the gate electrode is immersed. Sometimes, the gate electrode is an external electrode that is often integrated in the same plane as the source and drain electrodes (coplanar structures), as considered in this work. The most widely used polymer is p-type conductive poly(3,4-ethylenedioxythiophene) doped with poly(styrene sulfonate) (PEDOT:PSS). When a source–drain voltage (V_d) is applied, a drain current (I_d) flows through the channel. The current in the channel is controlled by the gate voltage (V_g). Upon application of a positive gate voltage, the cations in the electrolyte are injected into the PEDOT:PSS channel, which leads to a decrease in the hole concentration and a reduction in the conductivity of PEDOT. This will deplete the number of available carriers, meaning that the drain–source current decreases.

The electrical response of an OECT is therefore determined by the interaction between the ionic and electronic charge carriers, and specific models therefore need to be developed.

Since the conducting polymer used as the channel for the device is amorphous, the drift-diffusion transport mechanism in OECTs [5] is conditioned by hopping, a thermally assisted quantum mechanical tunneling process that is much slower than transport through organic crystals [6], [7]. This gives rise to a dependence on the carrier concentration for carrier mobility. In addition, the cations injected into the PEDOT:PSS layer move along the channel toward the drain contact before establishing a steady-state condition, making a 2-D description of OECTs necessary [8] (the ion transport is currently assumed to be vertical to the transistor channel, which is modeled with a gate capacitance).

The fact is that a nonmonotonic dependence of the transconductance on the gate voltage therefore results, including a peak transconductance, which makes modeling of this effect difficult.

For simplicity, the dc characteristics of OECTs are usually modeled based on the assumption of a MOSFET-like response [2], [9], [10]. Some empirical corrections to the drain current in the linear regime were made in [11]; in other studies, models have incorporated the mobility and gate capacitance depending on carrier concentration [12], [13], [14]. In any case, the use of a gradual channel approximation does not allow for predictions of the peak transconductance without giving rise to inconsistency in some of the remaining dc characteristics. To try to overcome this, a piecewise linear function for the transconductance was proposed in [15], but a plateau for transconductance rather than a peak value was the result. Bonafè et al. [16] have had to assume an unrealistic gate-voltage-dependent contact resistance at the drain terminal.

DC numerical simulations of these transistors have been performed based on the assumption of drift-diffusion transport [8], [17], but unrealistic transconductance plateaus have again resulted. Numerical solutions are also required with some physical models in which the geometry of the internal fluidic circuits of the system can change over time [18]. The simulation of OECT-based circuits therefore remains a challenge, due to the absence of accurate mathematical models.

In biosensing applications, the OECT current is modulated by the concentration of a given electroactive species in the electrolyte solution (e.g., glucose concentration). The current variation was modeled by Bernards et al. [19] by introducing an effective gate voltage in which a voltage offset was added to the gate voltage as a function of the concentration. The current variation was then proportional to the transconductance.

In this work, we aim to predict the evolution of the peak transconductance of OECTs for biosensing applications and a compact model is proposed that stands out in terms of its simplicity and rapid determination of its parameters. A preliminary discussion of charge transport in polymer semiconductors is given in Section II. The device under test (DUT) considered here and the experimental setup used for dc measurements are described in Sections III and IV, respectively. The dc model is introduced and compared to other models for OTFTs in Section V. Finally, the conclusions are presented in Section VI.

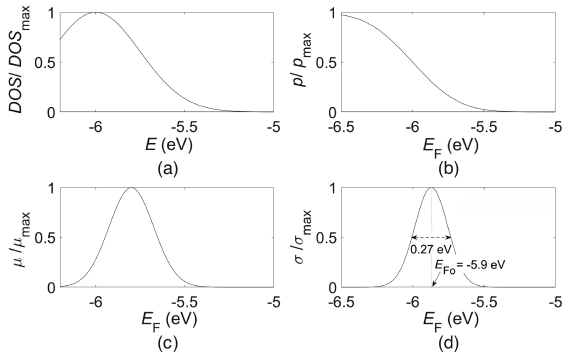

Fig. 2. (a) Normalized density of states, DOS/DOS$_{max}$, versus energy, from (1). (b) and (c) Normalized values of the hole concentration and hole mobility, p/p_{max} and μ/μ_{max}, versus Fermi level, from (2) and (3), respectively, with $p_{max} = p(E_F \rightarrow -\infty)$ and (d) resulting normalized conductivity, σ/σ_{max}; DOS$_{max} = 4 \times 10^{21}$ eV^{-1}·cm^{-3}, $E_o = -6$ eV, $c = 0.25$ eV, $\mu_{max} = 10^{-3}$ cm^2/V·s, $E_1 = -5.8$ eV, and $d = 0.12$ eV.

II. Preliminary Considerations

For PEDOT:PSS, a Gaussian-shaped energy density of state (DOS) results [17], [20], [21], [22]

$$\text{DOS} = \text{DOS}_{\text{max}} e^{-\frac{(E-E_o)^2}{2c^2}} \tag{1}$$

where DOS$_{max}$ is the peak height of the curve, E_o is the position of the center of the peak, and c is the standard deviation, with typical values of 4×10^{21} eV^{-1}·cm^{-3}, -6 eV, and 0.25 eV, respectively [23]. Fig. 2(a) shows the resulting energy distribution of the normalized density of states (DOS/DOS$_{max}$).

Using the Fermi–Dirac distribution, the hole concentration (p) is obtained as follows:

$$p = \int_{-\infty}^{+\infty} \frac{\text{DOS}}{1 + e^{\frac{E_F - E}{qV_T}}} dE \tag{2}$$

where E_F denotes the Fermi level, q is the elementary charge, and $V_T \approx 26$ mV is the thermal voltage at room temperature. The normalized result [p/p_{max}, where $p_{max} = p(E_F \rightarrow -\infty)$], which depends on the Fermi level, as depicted in Fig. 2(b), is evaluated by the fitting of the integrand with a 12th-order polynomial approximation, using the least-squares method, and performing the integral of the polynomial analytically for each value of the Fermi level. Note that two asymptotic values for the hole concentration are observed as follows:

1) p_{max}, representing the initial hole density in the PEDOT layer, which corresponds to the hole density in the channel of an OECT depleted of cations, with anions fixed within the electrolyte since the transistor predominantly operates in depletion mode [8].
2) Zero. That is, no hole concentration in the channel of a fully de-doped OECT, for a sufficiently high cationic charge leveraged from the electrolyte.

Due to the tunneling processes involved, the energy distribution of the PEDOT hole mobility (μ) follows that of the density of states. At low energies, a limited number of carriers populate the low density of states, and hopping between carrier sites is unlikely, resulting in low hole mobility. As the hole concentration increases (with a larger density of states), carriers fill higher energy sites, hopping is faster, and

the hole mobility rises. Finally, for large carrier densities, the density of states starts to reduce, meaning that hopping again becomes unlikely and the carrier mobility decreases [10], [21]. The charge carrier mobility is therefore dependent on the carrier concentration (i.e., the Fermi level), as experimentally observed in [10] and [21], and the dependence of the hole mobility on the Fermi level can be expressed as follows:

$$\mu = \mu_{\max} e^{-\frac{(E_F - E_1)^2}{2d^2}} \tag{3}$$

with typical values for the peak mobility ($\mu_{\max}$), the position of the center of the peak (E_1), and standard deviation (d) of 10^{-3} cm^2/V·s [17], −5.8 eV [21], and 0.12 eV [20], respectively. This dependence is depicted in Fig. 2(c) based on normalized values ($\mu/\mu_{\max}$).

When the hole concentration and hole mobility are known, the PEDOT conductivity can be obtained as $\sigma = qp\mu$. This has a bell-shaped distribution with the Fermi level, as shown in Fig. 2(d), for normalized data ($\sigma/\sigma_{\max}$) and reported in [20].

For the PEDOT layer of the channel of an OECT, using the gradual channel approximation and integrating along the channel length, the drain current (I_d) can be expressed as follows:

$$-I_d = -\frac{WT}{L}\int_0^{V_d} qp\mu dV = -\frac{WT}{L}\int_0^{V_d} \sigma dV \tag{4}$$

where V is the channel voltage. Thus, for the saturation regime of transistor operation, with the saturation drain voltage ($V_{d,sat}$) given by $V_{d,sat} = V_g - V_{th}$, the drain current (I_{dsat}) is

$$-I_{d,sat} = -\frac{WT}{L}\int_0^{V_g - V_{th}} \sigma dV = \frac{WT}{qL}\int_{q(V_g+V_0)}^{q(V_{th}+V_0)} \sigma dE_F \tag{5}$$

where $V_{th} = qp_{\max}/c_v$ is the threshold voltage (0.7 V) [9], with $c_v \approx 40$ F/cm^3 as the volumetric capacitance [24]; E_F is the Fermi level along the channel length, which is given by the following equation:

$$E_F = q(V_g - V + V_o) \tag{6}$$

with the channel voltages $V(0) = 0$ and $V(L) = V_g - V_{th}$ at the borders of the gate, by the source and drain side, respectively; $dV = -dE_F/q$; and $V_o = -6.2$ V is an offset potential related to the gate electrode material, the electrolyte composition, and the p-type doping concentration of PEDOT [5], [10].

By fitting the integrand by a Gaussian process regression model, the transfer characteristic in the saturation regime is evaluated using global adaptive quadrature and default error tolerances as shown in Fig. 3 (left axis) by a line for normalized data ($I_{d,sat}/I_{d,sat-max}$).

The dependence on the gate voltage of the transconductance in the saturation regime ($g_{m,sat}$), from the derivation of (5), is shown in Fig. 3 (right axis) by a line for normalized data ($g_{m,sat}/g_{m,sat-max}$). Note that the bell-shaped functions of $\sigma/\sigma_{\max}$ [with $E_F = q(V_g + V_o)$] and $g_{m,sat}/g_{m,sat-max}$ have the same width and position as the modes [with $E_{Fo} = q(V_{go} + V_o)$], which is indicated by open circles in Fig. 3. In addition, given that $\sigma_{\max} = g_{m,sat-max}/(WT/L) = 0.1$ S/cm, it is assumed that $g_{m,sat} = (WT/L)\cdot\sigma$ for dc modeling of OECTs.

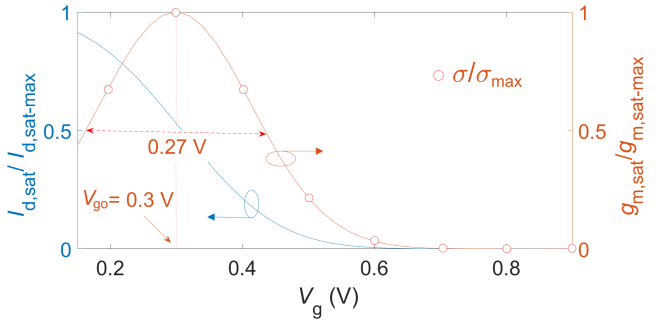

Fig. 3. Normalized values of the drain current (5) (left axis) and transconductance (right axis) versus gate voltage in the saturation regime; $V_{th} = 0.7$ V and $V_o = -6.2$ V.

It must be pointed out that this section is based on a mere description of the electrical parameters involved in the evaluation of the drain current in OECTs. In practice, the conductivity and hole concentration are determined before the hole mobility, which is derived as conductivity divided by the charge density of holes [20]. The reliability of mobility evaluation in organic field-effect transistors is a serious issue. In this respect, the use of the Y function method (YFM) seems promising [25].

III. Device Under Test

A thick-film OECT was manufactured for the test on a standard 1-mm-thick FR4 PCB substrate. The source, drain, and gate electrodes and the interconnections were manufactured using standard PCB manufacturers. In order to protect the Cu electrodes from corrosion, an electroless nickel immersion gold (ENIG) surface finish was applied, consisting of a two-layer metallic surface finish that included a thin layer of gold (2 μm) over a layer of nickel. The thickness of the traces was 35 μm. A resin layer was used to protect the interconnections, which were only open over the electrodes. A 3%–4% aqueous solution of high-conductivity-grade PEDOT:PSS was used to create the channel. The PEDOT:PSS was purchased from Sigma-Aldrich (reference 655201-25G). The gate electrode was protected by a tape, leaving only the channel region. The PEDOT was deposited over the channel by spinning at 1500 r/min for 30 s, and the channel was baked for 20 min at 100 °C and left to cool down to room temperature. Thereafter, the channel was conditioned by immersion for 2 h in a 10^{-2} M KCl solution with constant stirring. Finally, the system was rinsed three times with distilled water for 5 min.

The width (W), thickness (T), and length (L) of the channel were 5 mm, 25.5 μm, and 0.5 mm, respectively. The gold source/drain terminals had a size of 5 × 1 mm^2 and a 10.5 mm^2 gate electrode was used. The gap between the drain and gate electrodes (G) is 0.5 mm. The electrolyte consisted of a 0.1 M phosphate-buffered saline (PBS) solution with pH = 7.4 (P38135, Sigma-Aldrich), which is used typically in biosensing applications (e.g., glucose sensor). Fig. 4 shows the structure of the OECT and a SEM image of the channel. The thickness of the channel, T, is estimated by comparing it with the thickness of the electrode metallization (≈35 μm).

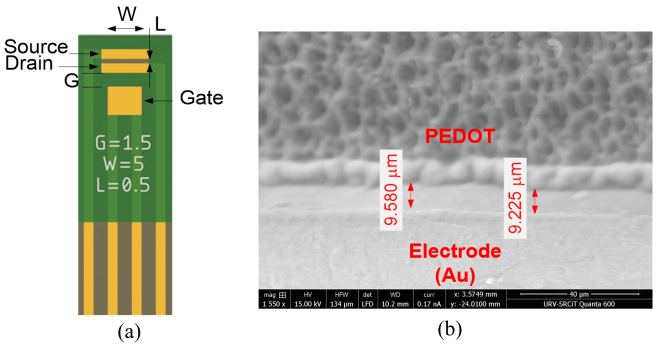

Fig. 4. (a) Image of the manufactured coplanar OECT with the main dimensions in mm. (b) SEM image of the channel indicating the distance from the edge of the electrode.

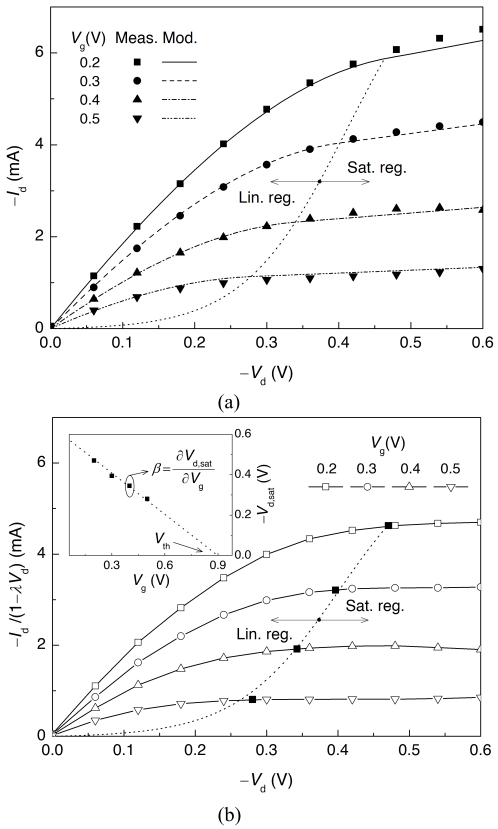

Fig. 5. (a) Measured (closed symbols) and modeled (lines) output characteristics for different gate voltages. (b) Ideal output characteristics (open symbols with a line) and extracted saturation drain voltages (closed symbols). The linear and saturation regimes are divided by the dotted line. Inset: dependence of the saturation drain voltage on the gate voltage. Extracted and modeled data are represented by closed symbols and the dotted line, respectively.

IV. Experimental Setup

The dc characteristics for gate voltages from 0.15 to 1 V, in steps of 0.05 V, and drain voltages from −0.6 to 0 V, in steps of 0.6 V, were obtained using a multimeter (Agilent 34401A). A power source (Keysight EDU36311A) was used for the biasing of the transistor. Data were acquired via instruments controlled by USB.

V. DC Model

Modeling starts from the measured output characteristics of the OECT, which are shown in Fig. 5(a) by closed symbols.

TABLE I
PARAMETERS OF THE DC MODEL

λ (V^{-1})	V_{go} (V)	σ_{max} (S/cm)	ΔV_{go} (V)	V_{th} (V)	β (-)
0.65	0.30	0.54	0.21	0.90	0.67

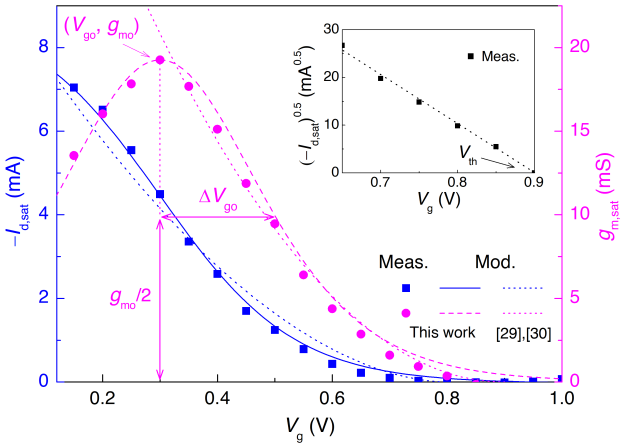

Fig. 6. Transfer characteristics (left axis) and transconductance versus gate voltage (right axis) in the saturation regime, for $V_d = -0.6$ V. Measured and modeled data are represented by closed symbols and lines, respectively. Inset: threshold voltage extraction. Measured and modeled data are represented by closed symbols and the dotted line, respectively.

Ideal output characteristics (with zero output conductance in saturation regime) result from dividing the measured drain current by $(1 - \lambda V_d)$, where λ is the channel-length modulation coefficient [14], which could be associated with effects from fringing capacitances at the surface of the channel [26]; its value is indicated in Table I. The ideal output characteristics are shown in Fig. 5(b) by open symbols with a line.

The measured transfer characteristics in the saturation regime (for $V_d = -0.6$ V) and the resulting gate voltage dependence of the transconductance are shown by closed symbols in Fig. 6 (left and right axes, respectively). As previously mentioned, a bell-shaped dependence for the transconductance is observed. Considering that $g_{m,sat}/(1 - \lambda V_d) = (WT/L) \cdot \sigma$ and given that there is no elementary indefinite integral for a Gaussian function, the derivative of the sigmoid function used for $g_{m,sat}$ is as follows:

$$g_{m,sat} = g_{mo} \cdot \frac{4 \cdot e^{\frac{V_g - V_{go}}{\alpha \Delta V_{go}}}}{\left(1 + e^{\frac{V_g - V_{go}}{\alpha \Delta V_{go}}}\right)^2} \tag{7}$$

where α is set to 0.567 so that $g_{m,sat}/g_{mo} = 0.5$ for $V_g = V_{go} + \Delta V_{go}$; ΔV_{go} accounts for the transconductance deviation; $g_{mo} = \sigma_{max} WT(1 - \lambda V_d)/L$ is the peak transconductance for the gate voltage V_{go}; and the maximum conductivity, σ_{max}, depends on the doping concentration and mobility of PEDOT. Values for V_{go} and σ_{max} are obtained from the measured peak transconductance and ΔV_{go} by adjusting the measured transconductance characteristic using the least-squares method; they are listed in Table I.

The modeled dependence on the gate voltage of the transconductance in the saturation regime is shown in Fig. 6 (right axis) by a dashed line, and good agreement with the measured data, which are shown by closed symbols, is found. By integrating $g_{m,sat}$ in (7) and since $I_{d,sat}$ ($V_g = V_{th}$) = 0, the drain current in the saturation regime is obtained as follows:

$$-I_{d,sat} = 4a\Delta V_{go} g_{mo} \cdot \left(\frac{1}{1+e^{\frac{V_g - V_{go}}{a\Delta V_{go}}}} - \frac{1}{1+e^{\frac{V_{th} - V_{go}}{a\Delta V_{go}}}} \right). \quad (8)$$

As illustrated in the inset to Fig. 6, V_{th} is determined in the vicinity of the cut-off region from the gate voltage axis intercept of the resulting $(-I_{d,sat})^{0.5}$–V_g linear regression [27]; its value is shown in Table I. The resulting modeled transfer characteristic in the saturation regime is shown in Fig. 6 (left axis) by a solid line. Again, good agreement with the corresponding measured data, which are shown by closed symbols, is achieved.

When the drain voltage reduces, a lower longitudinal electric field causes the drain current due to hopping to diminish [23], [28]. In addition, fewer cations in the channel move toward the drain contact. Hence, once the saturation regime is determined, the linear regime is modeled based on the assumption of the gradual channel approximation [9] and constant mobility and gate capacitance. The drain current, $I_{d,lin}$, is written as follows:

$$I_{d,lin} = I_{d,sat} \cdot \left[1 - \left(\frac{V_d - V_{d,sat}}{V_{d,sat}} \right)^2 \right] \quad (9)$$

which is valid for $V_d > V_{d,sat}$, the saturation drain voltage necessary to pinch off the channel at the drain. The expression in (9) ensures continuity between the linear and saturation regimes of not only the drain current but also the transconductance and output conductance, regardless of the dependence of $V_{d,sat}$ on the gate voltage. The saturation drain voltages are extracted from the ideal output characteristics, as shown in Fig. 5(b) when transitioning between the saturation and linear regimes; these data are represented in Fig. 5(b) by closed symbols. A linear dependence of the saturation drain voltage on the gate voltage is observed, as shown in the inset to Fig. 5(b) by the dotted line. As the saturation drain voltage is zero when the gate voltage equals V_{th}, $V_{d,sat}$ is given by the following equation:

$$V_{d,sat} = \beta \cdot (V_g - V_{th}) \quad (10)$$

where β is a fitting parameter obtained by linear regression (see Table I). It should be noted that for an OECT, β is lower than unity (the value for MOSFETs), which is in agreement with experimental data reported in [14]. This could be attributed to the fact that cations are injected from the electrolyte into the OECT, which move along the channel toward the drain contact, thus reducing the required drain voltage at which the channel pinches off [8].

By solving (10) for V_g and substituting it into (8), the modeled I_d–$V_{d,sat}$ characteristic that separates the linear and saturation regimes can be derived. This is represented by a dotted line in Fig. 5(a), and the corresponding ideal curve is depicted in Fig. 5(b). Finally, based on (8)–(10), the output characteristics are successfully modeled shown by the lines in Fig. 5(a).

Compared to other models proposed for OTFTs in the literature, the current model allows us to reproduce the maximum transconductance. For the dependence of mobility on hole concentration, it is usually assumed that $\mu \propto p^{\gamma}$ [29], [30] (the mobility enhancement factor, γ, is zero in the original model proposed by Bernards and Malliaras [9]). Then, the drain current and transconductance in the saturation regime are given, respectively, by the following equations:

$$-I_{d,sat} = \frac{K}{\gamma+2} \cdot (V_{th} - V_g)^{\gamma+2} (1 - \lambda V_d) \quad (11)$$

and

$$g_{m,sat} = K \cdot (V_{th} - V_g)^{\gamma+1} (1 - \lambda V_d) \quad (12)$$

where K groups the geometric and rest of technological bias-independent parameters. In this case, only the minimum for $g_{m,sat}$ (zero) when the transistor is turned off can be predicted. The resulting modeled data are represented in Fig. 6 by dotted lines. Note how the peak of the transconductance observed experimentally cannot be modeled (with $K = 41.12$ mA/V$^{\gamma+2}$ and $\gamma = 1.02$). The origin of the problem is the assumption for exponential DOS in the above (and other) model(s) of OTFTs, which results in a power-law enhancement of mobility with gate bias through the mobility enhancement factor.

Accordingly, in cases when bell-shaped DOS, channel current, or transconductance are observed, the proposed model should replace channel current models, e.g., the generic OTFT model in [29] and [30].

VI. Conclusion

A compact model of the dc characteristics of OECTs is proposed, which takes into account the nonmonotonic dependence of the transconductance on the gate voltage in the saturation regime. The typical peak transconductance of OECTs is also correctly predicted, which can be useful in future works for bio-sensing applications. The proposed model can be easily incorporated into circuit simulators, and extraction of the necessary parameters from the dc characteristics can be done in a straightforward way.

References

[1] X. Guo et al., "Organic electrochemical transistor for in situ detection of H_2O_2 released from adherent cells and its application in evaluating the in vitro cytotoxicity of nanomaterial," *Anal. Chem.*, vol. 92, no. 1, pp. 908–915, Jan. 2020, doi: 10.1021/acs.analchem.9b03718.

[2] A. Ait Yazza, P. Blondeau, and F. J. Andrade, "Simple approach for building high transconductance paper-based organic electrochemical transistor (OECT) for chemical sensing," *ACS Appl. Electron. Mater.*, vol. 3, no. 4, pp. 1886–1895, Apr. 2021, doi: 10.1021/acsaelm.1c00116.

[3] S. E. Doris, A. Pierre, and R. A. Street, "Dynamic and tunable threshold voltage in organic electrochemical transistors," *Adv. Mater.*, vol. 30, no. 15, Apr. 2018, Art. no. 1706757, doi: 10.1002/adma.201706757.

[4] Y. van de Burgt et al., "A non-volatile organic electrochemical device as a low-voltage artificial synapse for neuromorphic computing," *Nature Mater.*, vol. 16, no. 4, pp. 414–418, Apr. 2017, doi: 10.1038/NMAT4856.

[5] K. Tybrandt, I. V. Zozoulenko, and M. Berggren, "Chemical potential–electric double layer coupling in conjugated polymer–polyelectrolyte blends," *Sci. Adv.*, vol. 3, no. 12, Dec. 2017, Art. no. eaao3659, doi: 10.1126/sciadv.aao3659.

[6] A. B. Kaiser and V. Skákalová, "Electronic conduction in polymers, carbon nanotubes and graphene," *Chem. Soc. Rev.*, vol. 40, no. 7, p. 3786, Jul. 2011, doi: 10.1039/c0cs00103a.

[7] O. Marinov, M. J. Deen, J. A. Jiménez-Tejada, and C. H. Chen, "Variable-range hopping charge transport in organic thin-film transistors," *Phys. Rep.*, vol. 844, pp. 1–105, Feb. 2020, doi: 10.1016/j.physrep.2019.12.002.

[8] P. R. Paudel, V. Kaphle, D. Dahal, R. K. Radha Krishnan, and B. Lüssem, "Tuning the transconductance of organic electrochemical transistors," *Adv. Funct. Mater.*, vol. 31, no. 3, Jan. 2021, Art. no. 1616301X, doi: 10.1002/adfm.202004939.

[9] D. A. Bernards and G. G. Malliaras, "Steady-state and transient behavior of organic electrochemical transistors," *Adv. Funct. Mater.*, vol. 17, no. 17, pp. 3538–3544, Nov. 2007.

[10] J. T. Friedlein, R. R. McLeod, and J. Rivnay, "Device physics of organic electrochemical transistors," *Organ. Electron.*, vol. 63, pp. 398–414, Dec. 2018.

[11] F. F. Hanzaee et al., "A DC model for organic electrochemical transistors and analysis of their performance as voltage amplifiers," in *Proc. IEEE Int. Midwest Symp. Circuits Syst. (MWSCAS)*, Lansing, MI, USA, Aug. 2021, pp. 275–278, doi: 10.1109/MWSCAS47672.2021.9531818.

[12] R. Colucci, H. F. D. P. Barbosa, F. Günther, P. Cavassin, and G. C. Faria, "Recent advances in modeling organic electrochemical transistors," *Flexible Printed Electron.*, vol. 5, no. 1, Jan. 2020, Art. no. 013001, doi: 10.1088/2058-8585/ab601b.

[13] J. T. Friedlein, S. E. Shaheen, G. G. Malliaras, and R. R. McLeod, "Optical measurements revealing nonuniform hole mobility in organic electrochemical transistors," *Adv. Electron. Mater.*, vol. 1, no. 11, Nov. 2015, Art. no. 1500189, doi: 10.1002/aelm.201500189.

[14] D. Tu, L. Herlogsson, L. Kergoat, X. Crispin, M. Berggren, and R. Forchheimer, "A static model for electrolyte-gated organic field-effect transistors," *IEEE Trans. Electron Devices*, vol. 58, no. 10, pp. 3574–3582, Oct. 2011, doi: 10.1109/TED.2011.2162648.

[15] J. Nissa, P. Janson, D. T. Simon, and M. Berggren, "Expanding the understanding of organic electrochemical transistor function," *Appl. Phys. Lett.*, vol. 118, no. 5, Feb. 2021, Art. no. 053301, doi: 10.1063/5.0039345.

[16] F. Bonafè, F. Decataldo, B. Fraboni, and T. Cramer, "Charge carrier mobility in organic mixed ionic–electronic conductors by the electrolyte-gated van der Pauw method," *Adv. Electron. Mater.*, vol. 7, no. 10, Oct. 2021, Art. no. 2100086, doi: 10.1002/aelm.202100086.

[17] M. Koch et al., "Device physics, modeling and simulation of organic electrochemical transistors," *IEEE J. Electron Devices Soc.*, vol. 11, no. 2, pp. 665–671, Sep. 2023, doi: 10.1109/JEDS.2023.3263278.

[18] F. Gentile, F. Vurro, F. Picelli, M. Bettelli, A. Zappettini, and N. Coppedè, "A mathematical model of OECTs with variable internal geometry," *Sens. Actuators A, Phys.*, vol. 304, Apr. 2020, Art. no. 111894, doi: 10.1016/j.sna.2020.111894.

[19] D. A. Bernards, D. J. Macaya, M. Nikolou, J. A. DeFranco, S. Takamatsu, and G. G. Malliaras, "Enzymatic sensing with organic electrochemical transistors," *J. Mater. Chem.*, vol. 18, no. 1, pp. 116–120, 2008.

[20] J. T. Friedlein et al., "Influence of disorder on transfer characteristics of organic electrochemical transistors," *Appl. Phys. Lett.*, vol. 111, no. 2, Jul. 2017, Art. no. 023301, doi: 10.1063/1.4993776.

[21] B. D. Paulsen and C. D. Frisbie, "Dependence of conductivity on charge density and electrochemical potential in polymer semiconductors gated with ionic liquids," *J. Phys. Chem. C*, vol. 116, no. 4, pp. 3132–3141, Feb. 2012, doi: 10.1021/jp2093934.

[22] A. Abutaha et al., "Correlating charge and thermoelectric transport to paracrystallinity in conducting polymers," *Nature Commun.*, vol. 11, no. 1, Apr. 2020, Art. no. 1737, doi: 10.1038/s41467-020-15399-2.

[23] X. Shi et al., "Relating chain conformation to the density of states and charge transport in conjugated polymers: The role of the β-phase in poly(9,9-dioctylfluorene)," *Phys. Rev. X*, vol. 9, no. 2, May 2019, Art. no. 021038, doi: 10.1103/physrevx.9.021038.

[24] C. M. Proctor, J. Rivnay, and G. G. Malliaras, "Understanding volumetric capacitance in conducting polymers," *J. Polym. Sci. Part B, Polym. Phys.*, vol. 54, no. 15, pp. 1433–1436, Aug. 2016, doi: 10.1002/polb.24038.

[25] F. Huang et al., "Reliable mobility evaluation of organic field-effect transistors with different contact metals," *IEEE Electron Device Lett.*, vol. 40, no. 4, pp. 605–608, Apr. 2019, doi: 10.1109/LED.2019.2901315.

[26] O. Marinov, M. J. Deen, J. A. J. Tejada, and B. Iniguez, "Impact of the fringing capacitance at the back of thin-film transistors," *Organic Electron.*, vol. 12, no. 6, pp. 936–949, Jun. 2011, doi: 10.1016/j.orgel.2011.02.020.

[27] A. Ortiz-Conde, F. J. G. Sánchez, J. J. Liou, A. Cerdeira, M. Estrada, and Y. Yue, "A review of recent MOSFET threshold voltage extraction methods," *Microelectron. Rel.*, vol. 42, nos. 4–5, pp. 583–596, Apr. 2002.

[28] S. Marianer and B. I. Shklovskii, "Effective temperature of hopping electrons in a strong electric field," *Phys. Rev. B, Condens. Matter*, vol. 46, no. 20, pp. 13100–13103, Nov. 1992, doi: 10.1103/physrevb.46.13100.

[29] O. Marinov, M. J. Deen, U. Zschieschang, and H. Klauk, "Organic thin-film transistors: Part I—Compact DC modeling," *IEEE Trans. Electron Devices*, vol. 56, no. 12, pp. 2952–2961, Dec. 2009, doi: 10.1109/TED.2009.2033308.

[30] M. J. Deen, O. Marinov, U. Zschieschang, and H. Klauk, "Organic thin-film transistors: Part II—Parameter extraction," *IEEE Trans. Electron Devices*, vol. 56, no. 12, pp. 2962–2968, Dec. 2009, doi: 10.1109/TED.2009.2033309.